Mon. Not. R. Astron. Soc. **377,** 300–316 (2007) doi:10.1111/j.1365-2966.2007.11604.x

Young star clusters immersed in intermediate-age fields in the Small Magellanic Cloud

Andrés E. Piatti,[1⋆] Ata Sarajedini,[2⋆] Doug Geisler,[3⋆] David Clark[2⋆] and Juan Seguel[3⋆]

[1]*Instituto de Astronomía y Física del Espacio, CC 67, Suc. 28, 1428, Ciudad de Buenos Aires, Argentina*
[2]*Department of Astronomy, University of Florida, PO Box 112055, Gainesville, FL 32611, USA*
[3]*Grupo de Astronomía, Departamento de Física, Universidad de Concepción, Casilla 160-C, Concepción, Chile*

Accepted 2007 February 7. Received 2007 February 1; in original form 2006 October 19

ABSTRACT

We present CCD photometry in the Washington C and T_1 filters for six star clusters (B 34, NGC 256, NGC 265, NGC 294, IC 1611 and NGC 376) in the Small Magellanic Cloud (SMC) and their surrounding fields. The resultant colour–magnitude diagrams (CMDs) extend from $T_1 \sim 14$ to as faint as $T_1 \sim 22$ revealing the main-sequence turnoffs of the clusters. Adopting a metallicity of $Z = 0.004$, we compare our cluster photometry with theoretical isochrones in the Washington system in order to derive ages. To facilitate age determination of the surrounding fields, we use the magnitude difference between the helium-burning red clump stars and the main-sequence turnoff. Finally, we estimate mean metallicities for the field stars by comparing the location of the field red giant branch with standard giant branches for Galactic globular clusters of known abundance, corrected for age effects. Combining these results with our previous work, we find a clear trend of younger clusters being located closer to the centre of the SMC. In addition, there is a tendency for the mean metallicity and its dispersion to be greater inside 4° of the SMC's centre as compared to outside this radius. As far as the properties of the field stars are concerned, we find little correlation between the ages of the clusters and those of the field stars against which they are projected. Clearly, more work needs to be done to clarify these trends.

Key words: techniques: photometric – galaxies: individual: SMC – Magellanic Clouds – galaxies: star clusters.

1 INTRODUCTION

Studying the effect of interactions and mergers on the star formation histories of galaxies has gained renewed prominence over the last decade. This is largely due to the realization that large galaxies such as the Milky Way are built up through a process of fragmentation/disruption/accretion of smaller (dwarf) galaxies (Searle & Zinn 1978; Navarro, Frenk & White 1997; Font et al. 2006). While many investigators have studied distant galaxy systems as a means of understanding this process (Miley et al. 2006), the Milky Way–Large Magellanic Cloud (LMC)–Small Magellanic Cloud (SMC) system provides a nearby example that is especially scientifically profitable (Bekki et al. 2004; Bekki 2006). The relative proximity of these systems allows us to perform detailed age and abundance studies of individual field and cluster stars and thereby probe the star formation and chemical enrichment history of the Magellanic Clouds.

One of the most intriguing results of these studies has been that the star formation history of the SMC is quite different than that of the LMC. On the one hand, the age–metallicity relations of the LMC and SMC both reflect a 'bursting' (or episodic) star formation history (Pagel & Tautvaišienė 1998; Mighell, Sarajedini & French 2002; Piatti et al. 2002, 2005a). This could be a reflection of the past interaction history of the Milky Way, LMC and SMC (Bekki et al. 2004; Harris & Zaritsky 2004; Bekki 2006). On the other hand, the LMC appears to have had a more rapid initial chemical enrichment than that of the SMC. In addition, while the mean metallicity of the LMC has increased at a fairly modest rate over the past few Gyr (Grocholski et al. 2006), the SMC seems to have experienced a significantly more pronounced increase over the same time interval. A better determination of this behaviour during the past Gyr as manifested in the star clusters of the SMC is the primary focus of the present paper. The SMC exhibits one particularly important advantage over the LMC in this regard – it does not possess the infamous cluster age gap that the LMC clusters have which prevents

⋆E-mail: andres@iafe.uba.ar (AEP); ata@astro.ufl.edu (AS); dgeisler@astro-udec.cl (DG); dmclark@polaris.astro.ufl.edu (DC); jseguel@andromeda.cfm.udec.cl (JS)

Table 1. Observations log of selected clusters.

Star cluster[a]	α_{2000} (h m s)	δ_{2000} (° ′ ″)	l (°)	b (°)	Date	Filter	Exposure (s)	Airmass	Seeing (arcsec)
B 34, SMC OGLE 176	0 44 52	−73 00 07	303.60	−44.12	2002 October 28	*C*	2400	1.38	1.5
						R	800	1.40	1.5
					2002 October 30	*C*	240	1.30	1.6
						R	80	1.30	1.2
NGC 256, K 23, L 30, ESO 29-SC11	0 45 54	−73 30 24	303.47	−43.62	2002 October 29	*C*	2400	1.40	1.9
						R	800	1.60	1.3
					2002 October 30	*C*	240	1.30	1.6
						R	80	1.30	1.0
NGC 265, K 24, L 34, ESO 29-SC14	0 47 12	−73 28 38	303.35	−43.65	2002 October 29	*C*	2400	1.40	1.9
						R	800	1.60	1.3
					2002 October 30	*C*	240	1.30	1.6
						R	80	1.30	1.0
					2003 December 2	*C*	180	1.35	1.7
						R	60	1.35	1.5
NGC 294, L 47, ESO 29-SC22	0 53 06	−73 22 49	302.77	−43.75	2002 October 28	*C*	2400	1.37	1.8
						R	800	1.43	1.3
					2003 December 2	*C*	180	1.32	1.9
						R	60	1.32	1.5
IC 1611, K 40, L 61, ESO 29-SC27	0 59 48	−72 20 02	302.04	−44.78	2002 October 28	*C*	2400	1.36	1.6
						R	800	1.41	1.3
NGC 376, K 79, L 72, ESO 29-SC29	1 03 53	−72 49 34	301.65	−44.27	2002 October 30	*C*	2400	1.40	1.8
						R	800	1.43	1.2

[a]Cluster identifications are from Kron (1956, K), Lindsay (1958, L), Hodge & Wright (1974, HW), Lauberts (1982, ESO), Bica & Schmitt (1995, BS) and Pietrzyński et al. (1998, SMC OGLE).

the use of clusters from tracing the star formation and chemical evolution history of this galaxy over $\sim 1/2$ of its lifetime. The SMC has managed to both make and retain star clusters over essentially its entire lifetime, allowing the use of these prime probes for these purposes. In addition, the present-day metallicity of the SMC is substantially lower than that of the Galaxy or the LMC, allowing us to study star and cluster formation in a low-metallicity environment.

A number of other studies have examined the recent (i.e. $t \lesssim 1$ Gyr) star formation history of the SMC via its star clusters. Matteucci et al. (2002) present colour–magnitude diagrams (CMDs) for 10 young SMC clusters, although their primary focus is the field stellar populations of the SMC. They find evidence for a complex star formation history among the field stars and conclude that the metallicity of the old field stars is likely to be lower than the commonly adopted value of $Z = 0.004$.

Piatti et al. (2005a) present spectra for 18 SMC clusters of which 10 are younger than 1 Gyr. By comparing the line strengths and the shape of the continua with those of template clusters, they determine the age and metallicity of these SMC clusters. The spatial behaviour of these properties suggests that the clusters could have been formed in an outside-in fashion similar to a free-fall-like collapse. In addition, they find an intriguing coincidence between a burst of star formation exhibited by the field stars (Harris & Zaritsky 2004) and the star clusters of the inner SMC disc about 2.5 Gyr ago.

The most comprehensive study of the young clusters in the SMC appears to be that of Chiosi et al. (2006), who studied the ages of 311 clusters and 164 associations along with their field regions using isochrone comparisons in the CMD. They find a good correlation between the bursts in cluster and field star formation similar to what Piatti et al. (2005a) found. More importantly, Chiosi et al. (2006) also find a good correlation between these star formation episodes and the tidal interaction history of the Milky Way-LMC–SMC system. A more detailed examination, however, reveals some differences between the age properties of the clusters and field stars suggesting another mechanism is also influencing their formation.

In this paper, we continue our series (Piatti et al. 2002, 2005b) on the ages and metallicities of stellar populations in the SMC by presenting CMDs for six clusters and their surrounding fields. We seek to verify the results of Piatti et al. (2005a) and others with regard to the episodic nature of star formation in the SMC and its relation to the dynamical properties of the Milky Way–LMC–SMC system. The next section describes the observations and data reduction. Sections 3 and 4 present the CMDs of the clusters and their surrounding fields along with an analysis of their properties. The analysis is continued in Section 5 together with a discussion of the results and their implications. Our results are summarized in Section 6.

2 THE DATA

We selected six SMC clusters that had been the subject of an observational project aimed at enlarging the sample of well-studied star clusters in the SMC by obtaining CMDs down to below the main-sequence turnoff (MSTO) and thus derive their ages and metallicities. 10 of those observed clusters were recently studied by Piatti et al. (2005b). The present sample of clusters is given in Table 1, which lists their various designations, equatorial and Galactic coordinates and details of the observations. The observations were carried out during four nights with the Cerro Tololo Inter-American Observatory (CTIO) 0.9-m telescope in 2002 October and 2003 December with the Tektronix 2 K # 3 CCD, using quad-amp readout. The scale on the chip is 0.4 arcsec px^{-1}. The integrated IRAF[1]–ARCON 3.3 interface for direct imaging was employed as the data

[1] IRAF is distributed by the National Optical Astronomy Observatories, which is operated by the Association of Universities for Research in Astronomy, Inc., under contract with the National Science Foundations.

acquisition system. A mean gain of 3 e^-/ADU and a mean readout noise of 4.9 e^- resulted for the chosen settings.

We obtained data with the Washington (Canterna 1976) C and Kron–Cousins R filters. Geisler (1996) has shown that the R_{KC} filter is a very efficient substitute for the Washington T_1 filter and that $C - R$ accurately reproduces $C - T_1$ over at least the range $-0.2 \leqslant C - T_1 \leqslant 3.3$. We decided to use the Washington system because of its combination of broad-bands and high-metallicity sensitivity provided by the C filter, and the wide colour baseline between C and T_1. We also wished to maintain consistency with our previous studies in this series. Single exposures of 40 min in C and 800 s in R_{KC} were taken for each field. Additional short calibration exposures were taken on photometric nights for the clusters originally observed during non-photometric conditions.

Two of the nights (2002 October 30 and 2003 December 2) were photometric. On each photometric night, a significant number (typically 20) of standard stars from the list of Geisler (1996) were also observed. The airmasses of program objects were always $\leqslant$1.6 and the seeing was typically $\sim$1.5 arcsec, while for standard stars care was taken to cover a wide colour and airmass range in order to calibrate the program objects observed on these nights properly. The observations were supplemented with nightly exposures of bias, dome- and (when appropriate) twilight sky-flats to calibrate the CCD instrumental signature.

The CT_1 images were reduced at the Institute for Astronomy and Space Physics (Argentina) with IRAF using the QUADPROC package. The images were bias-subtracted and flat-fielded by employing weighted combined signal-calibration frames. In addition, we checked the chip for the existence of any illumination patterns; no correction was necessary. Then, the instrumental magnitudes for the standard fields were derived from aperture photometry using DAOPHOT/IRAF routines (Stetson et al. 1990), while those for the program stars were obtained through Point Spread Function (PSF) photometry using the stand-alone version of the DAOPHOT II/ALLSTAR package (Stetson 1994). We used least squares to simultaneously fit the relationships between instrumental and standard magnitudes for the nights of 2002 October 30 and 2003 December 2, and we obtained the following mean results:

$$c = (3.261 \pm 0.031) + C + (0.410 \pm 0.100) \times X_C - (0.110 \pm 0.013)\,(C - T_1), \quad (1)$$

$$r = (2.948 \pm 0.024) + T_1 + (0.160 \pm 0.010) \times X_R - (0.024 \pm 0.005)\,(C - T_1), \quad (2)$$

where X represents the effective airmass. The coefficients were derived through the IRAF routine FITPARAM. Capital and lowercase letters represent standard and instrumental magnitudes, respectively. The nightly rms errors from the transformation to the standard system were 0.017 and 0.013 mag for c and r, respectively, indicating these two nights were of excellent photometric quality.

The standard magnitudes and colours for all the measured stars of the clusters observed on 2002 October 30 and 2003 December 2 were calculated by inverting equations (1) and (2). For the remaining cluster observations, obtained on the non-photometric nights of 2002 October 28 and 29, we transformed their instrumental magnitudes and colours to the standard ones obtained from the short calibration observations taken on the photometric nights. In the case of IC 1611 – observed on 2002 October 28 only – we transformed the instrumental magnitudes and colours to standard values through the relations that arise for the cluster B 34 between the nights of 2002 October 28 and 30. Thus, the results for IC 1611 are on a more unsure photometric footing than are those for the other clusters.

Table 2. CCD CT_1 data of stars in the field of B 34.

Star	X (pixel)	Y (pixel)	T_1 (mag)	$\sigma(T_1)$ (mag)	$C - T_1$ (mag)	$\sigma(C - T_1)$ (mag)	N
...	...	...	...	...	...	...	...
874	931.332	140.168	20.086	0.030	1.430	0.066	1
875	297.250	140.182	20.908	0.128	−1.046	0.139	1
876	1009.304	140.370	17.728	0.000	−0.407	0.097	2
877	312.208	140.442	20.497	0.085	0.014	0.014	2
878	1504.135	140.467	18.298	0.004	1.729	0.020	2
...	...	...	...	...	...	...	...
...	...	...	...	...	...	...	...
...	...	...	...	...	...	...	...

Note. (X, Y) coordinates correspond to the reference system of Fig. 1. Magnitude and colour errors are the standard deviation of the mean, or else the observed photometric errors for stars with one measurement.

For clusters observed more than once, we combined all the independent measurements using the stand-alone DAOMATCH and DAOMASTER programs kindly provided by Peter Stetson. The final information gathered for each cluster of this paper consists of a running number per star, the x and y coordinates, the mean T_1 magnitudes and $C - T_1$ colours, the standard deviations – or the observational errors for stars observed once – $\sigma(T_1)$ and $\sigma(C - T_1)$ and the number of observations. We refer the readers to table 2 of Piatti et al. (2005b) for a listing of typical photometric errors for a single observation. These values are only representative and vary with cluster and field crowding, seeing, etc. Tables 2–7 give this information for B 34, NGC 256, NGC 265, NGC 294, IC 1611 and NGC 376, respectively. Only a portion of Table 2 is shown here for guidance regarding its form and content; the whole content of Table 2 is available in the online version of the *Journal on Synergy* (as are Tables 3–7) at http://www.blackwellpublishing.com/products/journals/suppmat/MNR/. In Fig. 1, we plot the distribution of the observed stars in the sky within $\approx$7 arcmin^2 around the cluster centres (the whole field of each image is of about 180 arcmin^2). The size of the plotting symbol is proportional to the T_1 brightness of the star.

The knowledge of the cluster central coordinates, the cluster density profiles and the main characteristics of their surrounding fields is valuable to disentangle the cluster features from those corresponding to the populous field. To determine the cluster central positions, we first counted the number of stars distributed along the x and y directions passing through the clusters and within strips of 150 pixels wide. The width of the strips was fixed so as to sample stars well beyond the clusters and, at the same time, to minimize the number of field stars, which only enhances the background level in the projected star density profiles. Likewise, the counts were done using intervals of 10, 20 and 40 pixels with the purpose of evaluating the influence of the involved spatial resolutions on the determination of cluster centres. Once the projected x and y distributions were obtained, we performed Gaussian fits using the NGAUSSFIT routine of the STSDAS IRAF package. We adopted a single Gaussian, and fixed the constant (i.e. stellar field densities assumed to be uniform) and linear terms to the corresponding background levels and to zero, respectively. The centre of the Gaussian, its amplitude and its full width at half-maximum (FWHM) acted as variables. We iterated the fitting procedure once on average, after eliminating a couple of discrepant points. The most important sources of uncertainty in

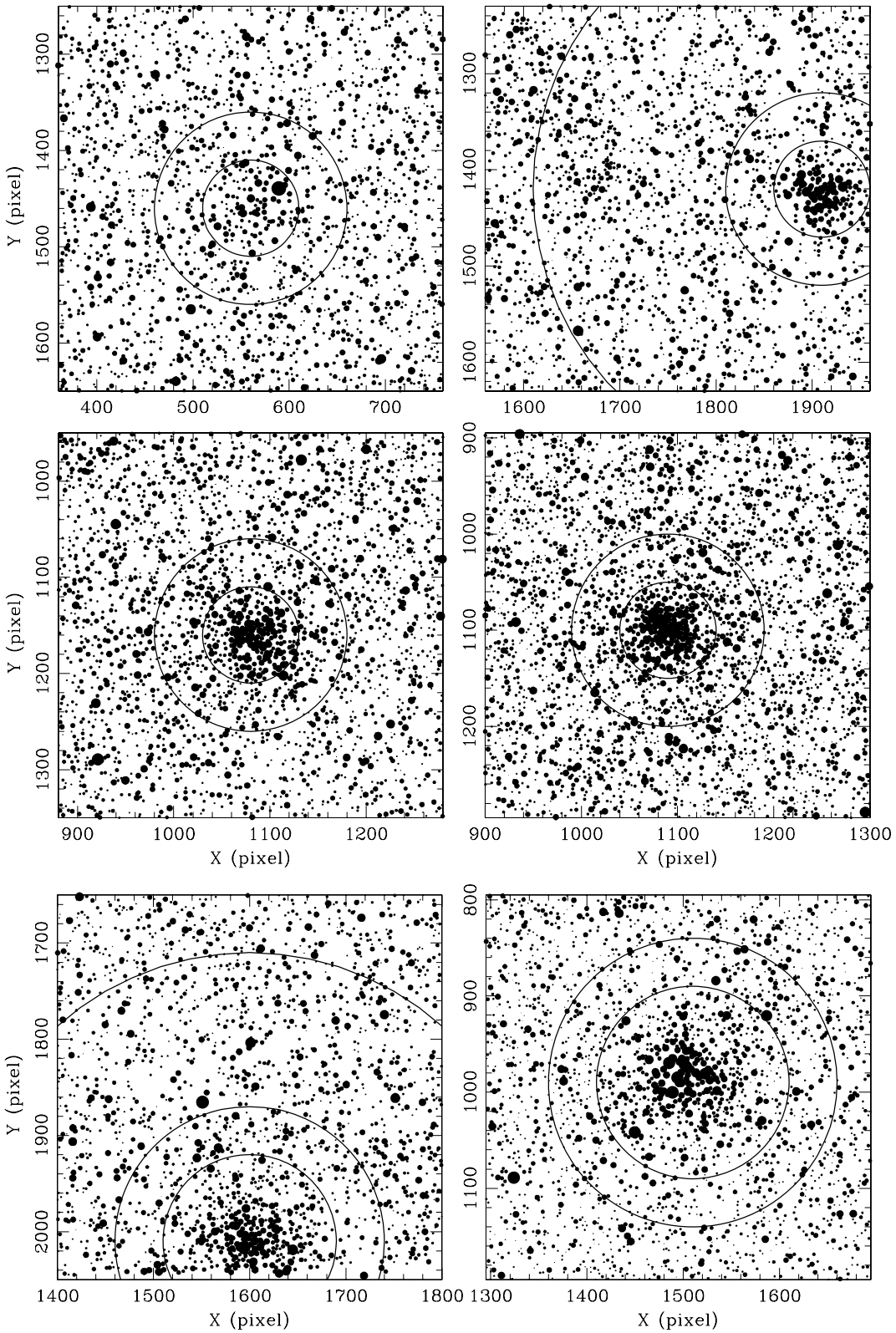

Figure 1. Schematic finding charts for the SMC cluster fields. B 34 (upper left), NGC 256 (upper right), NGC 265 (lower left) and NGC 294 (lower right). IC 1611 (middle left) and NGC 376 (middle right). Two or three concentric rings are generally shown, corresponding to the circular extractions explained in the text. North is up and east is to the left. The size of the plotting symbol is proportional to the T_1 brightness of the star.

the placement of cluster centres came from the relatively small ratio between the number of cluster and field stars, and the projected intracluster fluctuations due to both cluster and field star density variations. Cluster centres were finally determined with a standard deviation of ± 20 pixels in all cases.

We then built the cluster radial profiles, from which we estimated the cluster radii, which are generally used as indicators of the cluster dimensions, and established the areas over which field stars prevail. The availability of a field area is very important in order to separate the fiducial cluster sequence from that of the field and properly assess the field star contamination in the cluster CMD. Cluster stellar density radial profiles are usually built by counting the number of stars distributed in concentric rings around the cluster centre and normalizing the sum of stars in each ring to the unit area. This procedure allows us to stretch the radial profile to its largest possible extent, until the contained circle begins to fall outside our observed field. However, in order to move even farther away from the cluster centre, we decided to follow another method based on counts of stars located in boxes 20 pixels on a side, distributed throughout the field. Thus, the number of stars per unit area at a given radius r can be directly calculated through the expression

$$(n_{r+10} - n_{r-10}) \Big/ \left[(m_{r+10} - m_{r-10}) \times 20^2\right],$$

where n_j and m_j represent the number of counted stars and boxes included in a circle of radius j, respectively. Note that the method does not necessarily require a complete circle of radius r within the observed field to be able to estimate the mean stellar density at that distance. What is more, instead of having traced the radial profile of the clusters out to the radii of the largest complete circles that can be traced in the observed fields, we obtained cluster stellar density profiles that extend beyond the limits of the schematic finding charts (see Fig. 1).

The resulting density profiles are shown in Fig. 2. The latter show the number of stars per unit area expressed in pixels. The vertical straight lines indicate the radii of the circular extractions used to build the respective CMDs (see more details in Section 5). The background levels of all the fields are very similar ($\sim$0.01 stars pixels^{-2}), except in the case of NGC 265 and 294 whose background fields are one and a half times that value. As shown in Fig. 2, clusters are in general very small. Most of their stars lie within circles with radii of $\sim$50 pixels (20 arcsec) and they reach, on average, central stellar densities only two to three times higher than the surrounding fields.

We first examined the quality of our photometry in order to evaluate the influence of the photometric errors on the cluster fiducial characteristics on the CMDs. The T_1 magnitude and $C - T_1$ colour errors provided by DAOPHOT II for each cluster are shown in Fig. 3. We only plotted the errors for stars distributed within the innermost circular extractions, where cluster stars prevail. We recall that, due to the crowdedness in such areas, the photometric errors of these stars are generally larger than those for the observed field stars located further away. Even so, the mean magnitude and colour errors for stars brighter than $T_1 = 19$ are in the range $\langle\sigma(T_1)\rangle = 0.03$–$0.08$ and $\langle\sigma(C - T_1)\rangle = 0.03$–$0.09$, for stars with $T_1 = 19$–21, $\langle\sigma(T_1)\rangle \leqslant 0.15$ and $\langle\sigma(C - T_1)\rangle \leqslant 0.20$. Thus, the quality of our photometry allowed us to detect and measure the turn-off (TO) for all of the clusters, which was used in our age estimates. Indeed, by using the relation between the TO R magnitude and age according to theoretical isochrones by Lejeune & Schaerer (2001) and by comparing it with our data, we concluded that we are able to define TOs for stellar populations as old as 4.5 ± 1.0 Gyr ($R \approx 21.5$) with an error of 0.15 in R. Slightly fainter TOs can be reached at the expense of larger errors.

3 ANALYSIS OF THE CMDs

The relatively large size of the field of view allowed us not only to properly sample the entire extent of each cluster but also to sample a significant area of their surrounding field. We built several different circular extracted CMDs per cluster which are depicted in Figs 4 to 9. The figures contain separate panels for four different circular extractions which are labelled in pixels at the bottom right margins. The smallest circular extractions (upper left panels) were used to isolate predominantly cluster stars. They consist of very small areas given the generally small size of the clusters (see Fig. 2). Certainly, the innermost CMDs do not contain the whole cluster stellar population, but minimize the influence of field stars on their fiducial sequences. The most representative surrounding field CMDs, free from cluster contamination, are those built from the outermost circular extractions (bottom right panels), whose delimiting circles do not appear in Fig. 1, except for NGC 256 and IC 1611, because they encompass larger areas. These areas were chosen to lie well beyond the extent of the clusters. Finally, two extracted CMDs between the innermost and outermost CMDs were also included in the figures (upper right and bottom left panels), in order to show the transition from dominant cluster to field star CMDs. The choice of the various radii for each cluster was an iterative, slightly subjective process designed to obtain the best representation of the cluster and its transition to the field.

We estimate that the contamination of field stars in the extracted CMDs adjacent to the innermost ones varies between 60 and 90 per cent. The increasing presence of field stars in the CMDs adjacent to those of the smallest circular extractions is mainly due to field MS stars, which superimpose on the cluster MSs at their faintest portions or extend the cluster MS toward fainter magnitudes, as well as red giant clump (RGC) and red giant branch (RGB) stars of the SMC field. For this reason, and because of the relatively sharp density profiles, in the subsequent analysis we used the innermost extracted CMDs to represent the clusters. These still have some field star contamination which varies between 30 and 40 per cent.

B 34 (Fig. 4, upper left panel) seems to be an intermediate-age star cluster. Its TO and RGC are visible, as well as a well-delineated RGB. Note that the T_1 magnitude of the RGC ($\simeq$19) places the cluster – assumed to be around 1 Gyr old – at the nominal SMC distance (Piatti et al. 2001). While moving to the outer and spatially larger extractions, we observe a steady enhancement in the population of field stars in the cluster MS, RGC and RGB, respectively. This appearance in the cluster and field CMD features leads to the conclusion that both share similar ages, although the field clearly has some younger MS stars. Furthermore, we found that the resulting $r > 300$ pixel CMDs for the remaining five clusters (see bottom right panels of Figs 5–9) also have similar characteristics. This implies not only that all of the surrounding cluster fields are of similar ages ($\sim$1 Gyr), but also that this could be assumed as a representative age of the SMC inner disc – defined as the portion of the SMC disc with $a < 3\overset{\circ}{.}5$ – on to which all of the clusters are projected.

NGC 256 (Fig. 5, upper left panel) does not show any RGC, thus resulting in a cluster considerably younger than B 34. The relative youth of this cluster is also documented by its relatively vertical and bright MS. In the CMDs of the outer extractions, field features clearly arise. Note that this result repeats for all the cluster sample: the CMDs beyond the smallest circular extraction present, in increasing order, the MS and RGC of the SMC inner disc field.

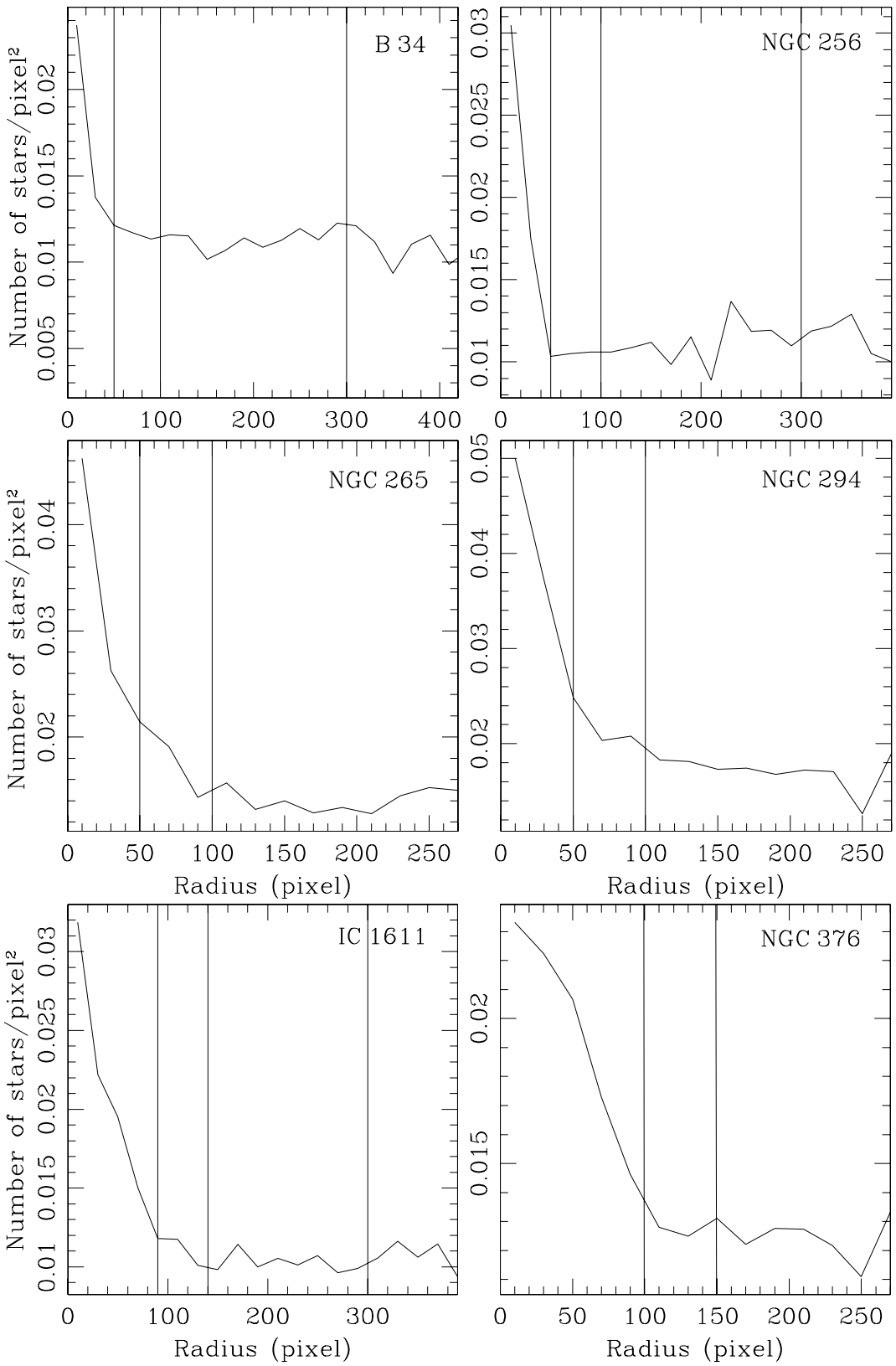

Figure 2. Density profiles for the selected clusters. Vertical straight lines indicate radii of the circular extractions used in the corresponding CMDs (see Section 3).

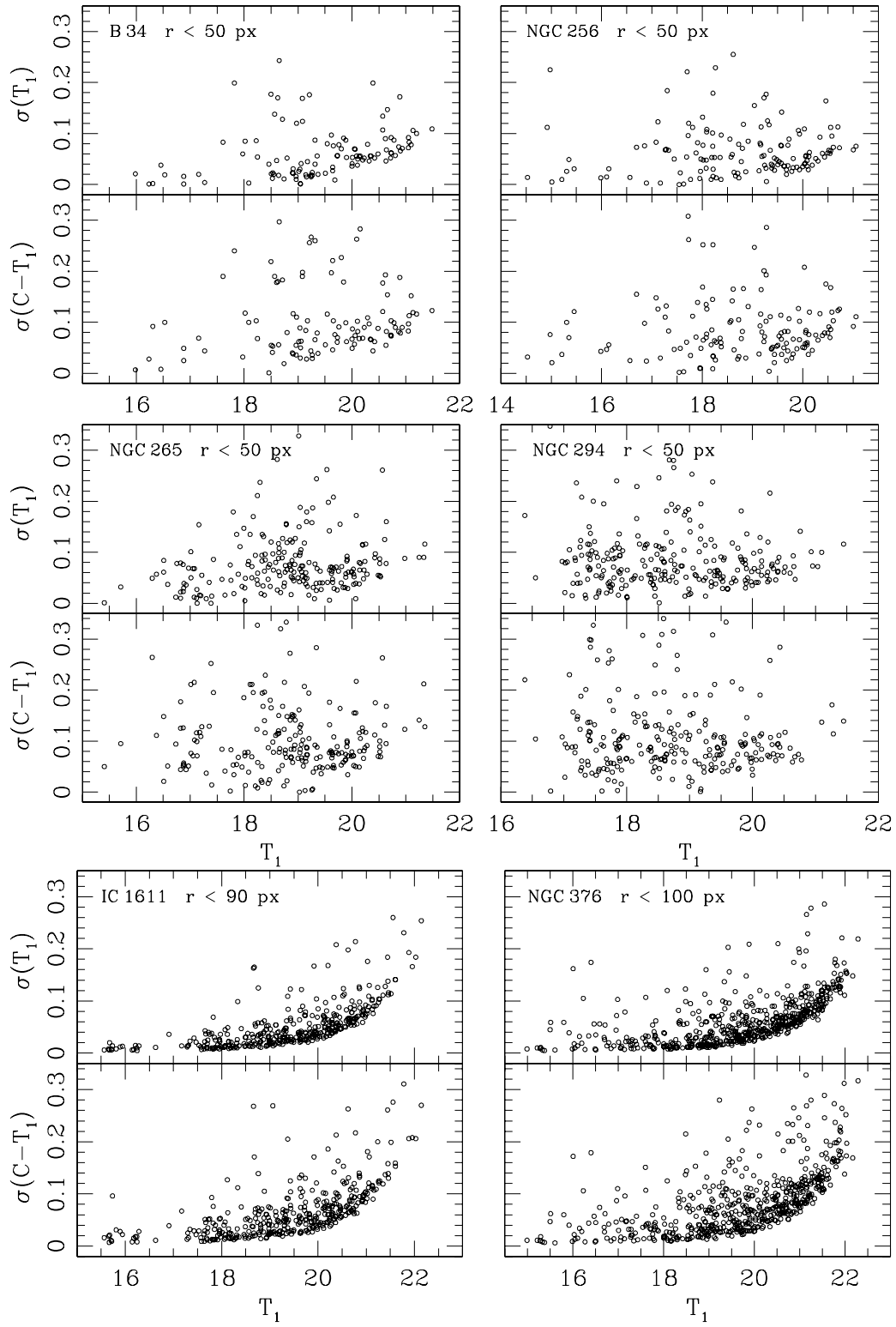

Figure 3. Magnitude and colour photometric errors as a function of T_1 for the innermost circular extractions of the associated clusters.

The CMD characteristics of NGC 265 (Fig. 6, upper left panel) are intermediate to the two previous clusters. It presents not only a relatively vertical and bright MS, but also a well-defined clump of blue loop stars at $T_1 \approx 17$. Therefore, we expect for the cluster age an intermediate value between those for NGC 256 and B 34. Likewise, NGC 294 also seems to be similar in age to NGC 265, as judged from its innermost extracted CMD (Fig. 7, upper left panel) which also includes a significant blue loop population, although with a higher colour dispersion.

IC 1611 (Fig. 8, upper left panel) and NGC 376 (Fig. 9, upper left panel) have well-populated vertical MSs covering ranges in T_1 from ∼4 up to 7 mag, respectively, which are clearly those of young

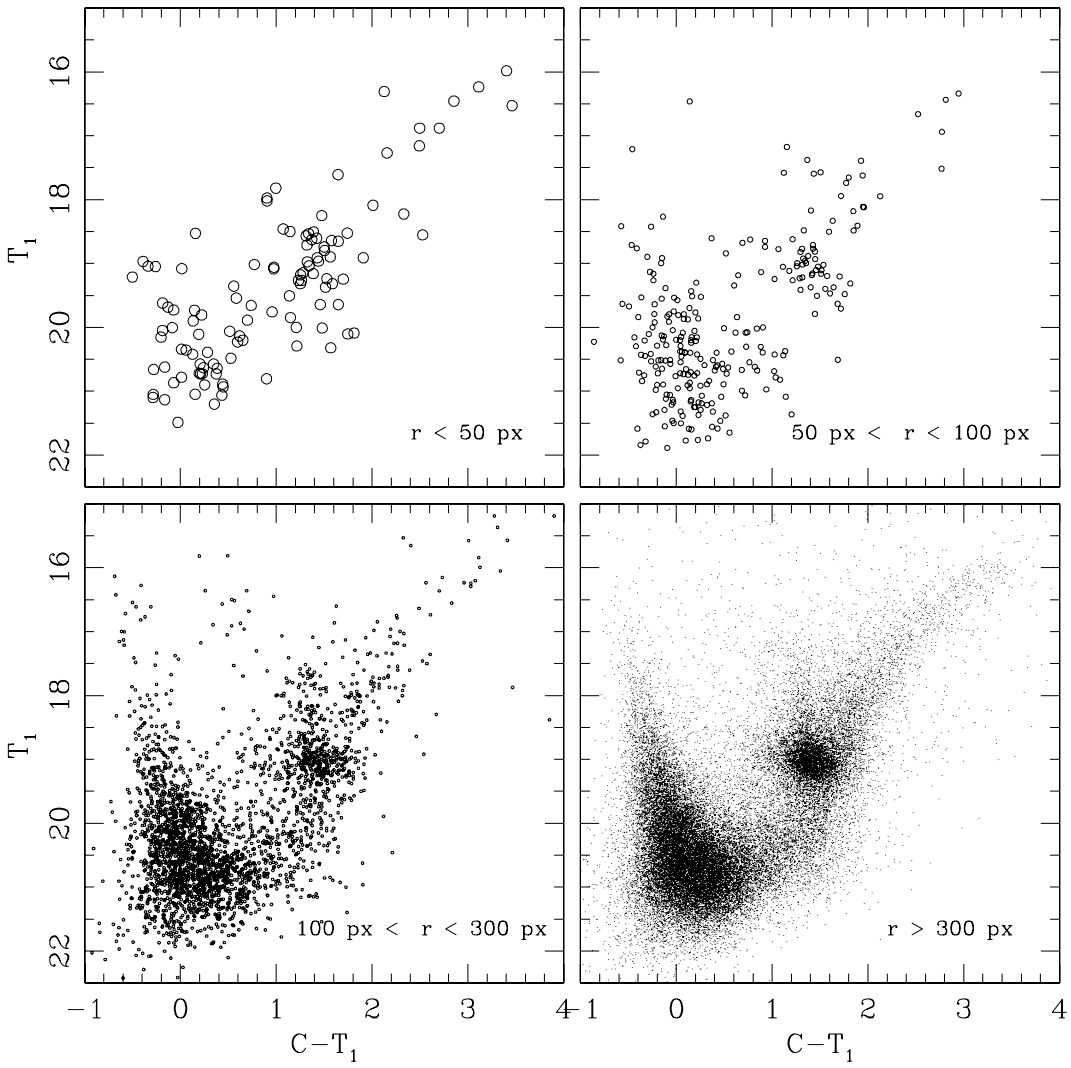

Figure 4. Washington T_1 versus $C - T_1$ CMDs for measured stars in the B 34 cluster field. Extraction radii in pixels are given in each panel.

clusters. One can infer from the presence of several evolved stars in the CMD of IC 1611 ($T_1 \sim 16$ mag) that this cluster is somewhat older than NGC 376. In both cases, a notable group of field RGC stars can be seen ($T_1 \sim 19$ mag).

4 CLUSTER AND FIELD FUNDAMENTAL PARAMETERS

It is well known that cluster metallicity plays an important role when estimating its age from the fit of theoretical isochrones. Indeed, theoretical isochrones with the same age but with different metallicities can range from slightly to remarkably different depending on their sensitivities to metallicity. For instance, the T_1 versus $C - T_1$ CMD has three times the metallicity sensitivity of the V versus $V - I$ CMD (Geisler & Sarajedini 1999) in terms of deriving the metallicity from the colour of the RGB. The distinction is particularly evident for the evolved phases of the RGC and RGB. As far as zero age main sequences (ZAMSs), they are often less affected by metallicity effects, and can even exhibit imperceptible variations for a specific metallicity range within the photometric errors. This is the case of the ZAMSs of SMC young to intermediate-age clusters, of the range we find for the present cluster sample (see below). In addition, the Washington RGB colour technique is strongly affected by age for clusters in this age range, requiring a large, age-dependent metallicity correction (Geisler et al. 2003). For these reasons, since there is no previous estimate of the cluster metal contents available, we simply adopted a representative value for SMC clusters younger than 2 Gyr, i.e. $Z = 0.004$ ([Fe/H] $= -0.7$; Piatti et al. 2005a).

Cluster reddening values were estimated by interpolating the extinction maps of Burstein & Heiles (1982, hereafter BH). BH maps were obtained from H I (21 cm) emission data for the southern sky and provide us with foreground $E(B - V)$ colour excesses which depend on the Galactic coordinates. More recently, Schlegel, Finkbeiner & Davis (1998, hereafter SFD) obtained full-sky maps from 100-μm dust emission. They found that at high latitudes, the dust map correlates well with maps of H I emission, but deviations are coherent in the sky and are especially conspicuous in regions of saturation of H I emission towards denser clouds and of formation of H_2 in molecular clouds. Since the $E(B - V)_{\rm SFD}$ values for half of our clusters are eight times higher than the $E(B - V)_{\rm BH}$ values, the SFD values are assumed to be saturated and we used the BH values for these inner disc clusters. We thus assume only foreground Galactic reddenings which do not allow for any reddening intrinsic to the SMC. Even still, the average of the BH values is 0.10 ± 0.05,

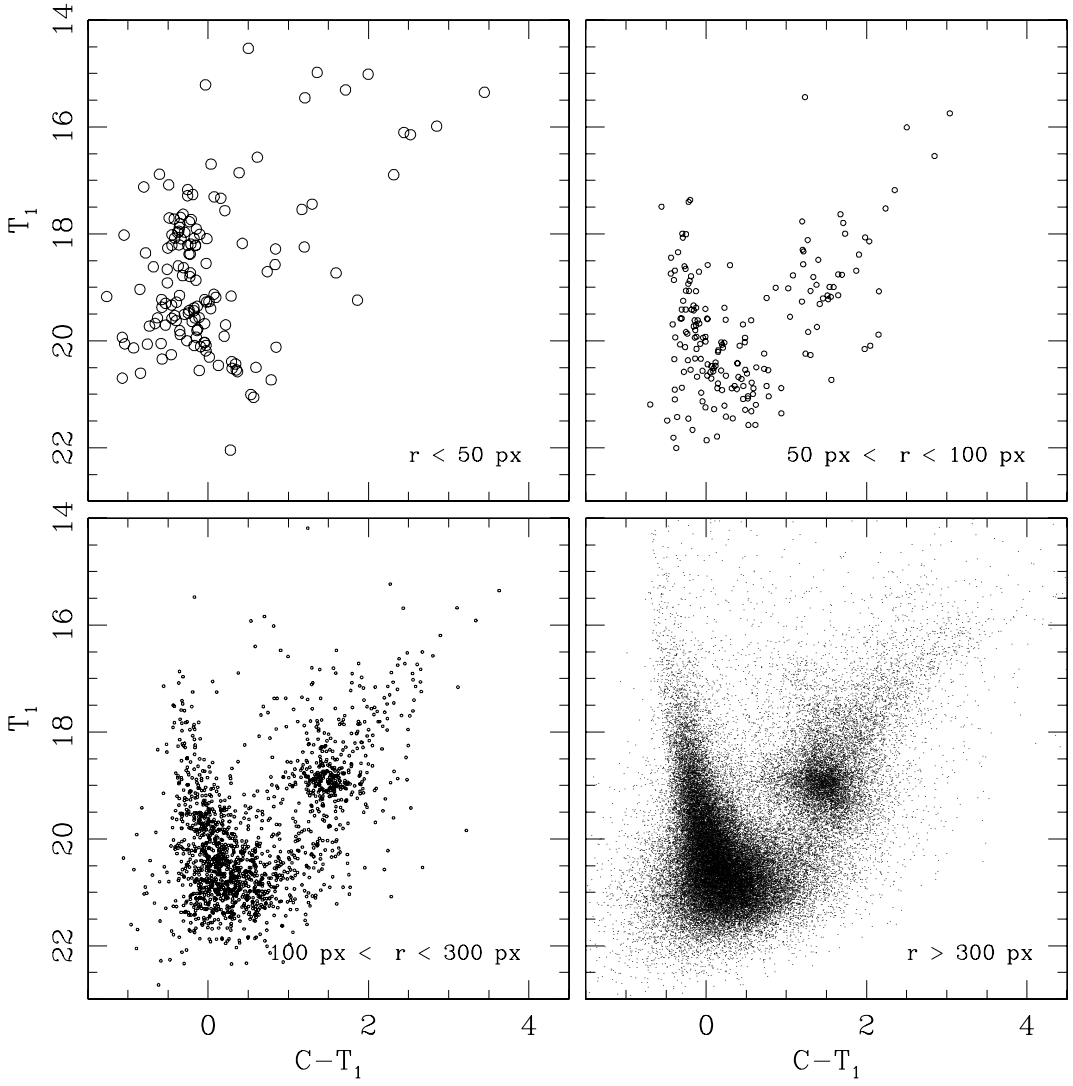

Figure 5. Washington T_1 versus $C - T_1$ CMDs for measured stars in the NGC 256 cluster field. Extraction radii in pixels are given in each panel.

while the typical reddening estimated by SFD for the SMC is 0.037. Table 8 lists the adopted $E(B - V)$ colour excesses.

As for the SMC distance modulus, we adopted for all the clusters the value of $(m - M)_o = 19.0$ obtained by Cioni et al. (2000) from the apparent bolometric magnitude determination of the tip of the RGB, using data extracted from the DENIS (Deep Near Infrared Survey of the Southern Sky) catalogue towards the Magellanic Clouds, and theoretical predictions. Crowl et al. (2001) found that, considering BH reddening values for populous SMC clusters, the line-of-sight depth of the galaxy is approximately 6 kpc. Then, bearing in mind that any cluster of the sample could be placed in front or behind the SMC, we conclude that the difference in its apparent distance modulus would be $\Delta(V - M_V) \sim 0.2$ mag, if a value of the order of 60 kpc is adopted for the SMC distance. Given that we estimate an uncertainty of 0.2–0.3 mag in adjusting ZAMSs to the cluster CMDs, our simple assumption of adopting a unique value for the distance modulus for all of the clusters should not affect the error budget in our final results substantially.

We derived ages of the cluster sample by fitting theoretical isochrones computed by Lejeune & Schaerer (2001, hereafter LS) to the cluster CMDs. LS calculated these isochrones using an updated version of the empirically and semi-empirically calibrated *BaSel* library of synthetic spectra (Lejeune, Cuisinier & Buser 1997, 1998). Their isochrone set for the age and metallicity ranges of our cluster sample shows no significant differences with those of Girardi et al. (2002) in the shape of the MSs or in the positions of the TOs and RGCs, and the agreement is very satisfactory. For the sake of uniformity with previous studies (Piatti et al. 2002, 2003a; Geisler et al. 2003), we decided to use the set of LS for $Z = 0.004$ computed taking into account overshooting effects.

To enter these isochrones in the observed cluster CMDs, the cluster reddenings and apparent distance modulus are needed. We then selected a set of isochrones, along with the equations $E(C - T_1) = 1.97E(B - V)$ and $M_{T_1} = T_1 + 0.58E(B - V) - (V - M_V)$ (Geisler & Sarajedini 1999), and superimposed them on the cluster CMDs, once they were properly shifted by the corresponding $E(B - V)$ colour excess and SMC apparent distance modulus. In the matching procedure, we commonly employed five different isochrones, ranging from slightly younger to slightly older than the derived cluster age. Fig. 10 shows the results of the fittings. For each cluster CMD, we plot the ZAMS and the isochrone of the adopted cluster age in

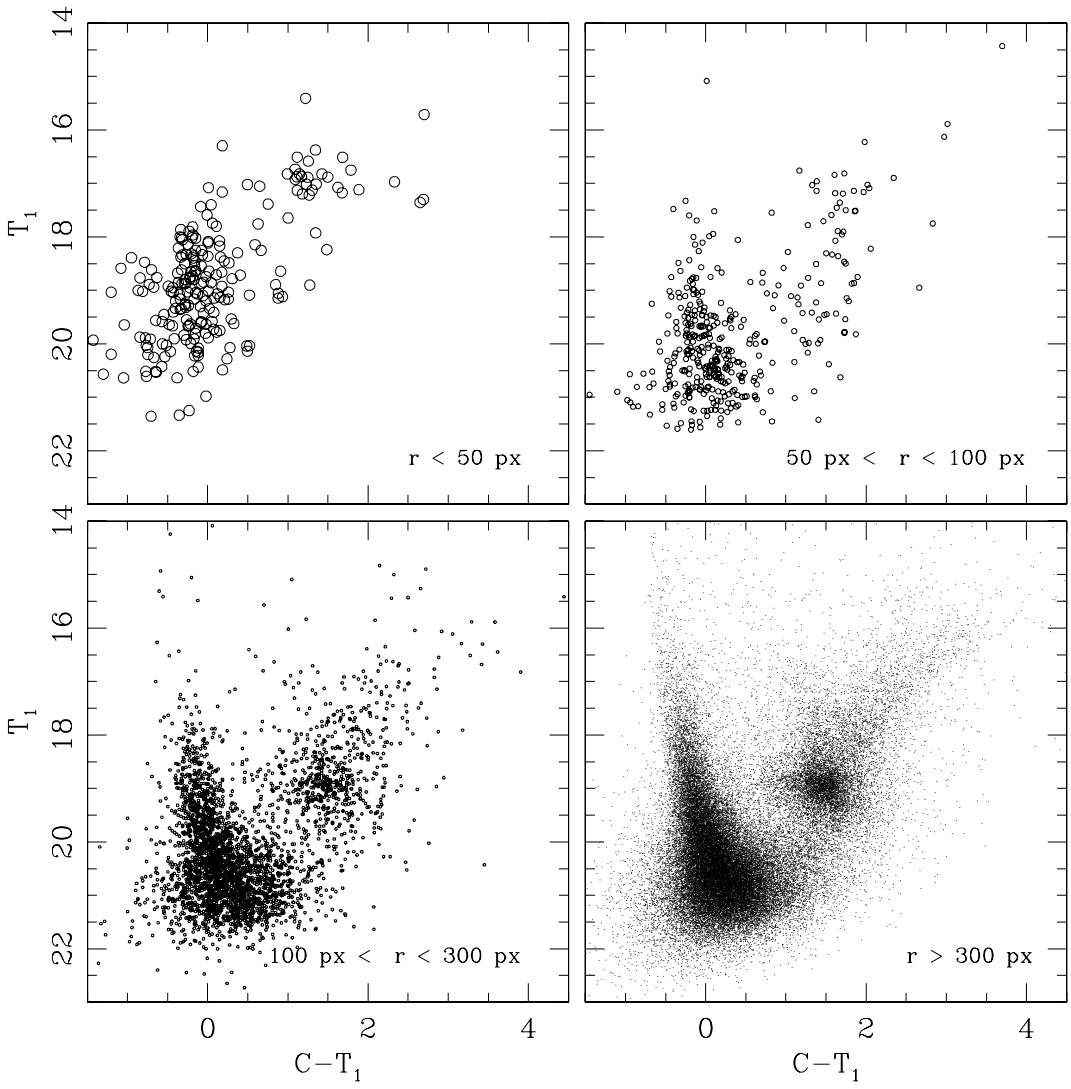

Figure 6. Washington T_1 versus $C - T_1$ CMDs for measured stars in the NGC 265 cluster field. Extraction radii in pixels are given in each panel.

solid lines, and two additional isochrones bracketing the derived age in dotted lines. Log t of the depicted isochrones are labelled at the bottom right margin of each panel. The ages of the bracketing isochrones were estimated by taking into account the estimated uncertainty in the colour excess and apparent distance modulus of 0.05 and 0.25 mag, respectively. The final ages for the cluster sample and their estimated errors are listed in Table 8.

The presence of RGCs and/or RGBs in the cluster CMDs made the fitting procedure easier. We noted, however, that the theoretically computed bluest stage during the He-burning core phase is redder than the observed RGCs in the CMDs of NGC 265 and 294, a behaviour which has also been detected in other studies of Galactic and Magellanic Cloud clusters (Geisler et al. 2003; Piatti, Clariá & Ahumada 2004a,b, for example). A similar result was found from the fitting of isochrones in the M_V versus $(V - I)_o$ diagram (among others Piatti, Clariá & Ahumada 2003b; Piatti et al. 2003c).

We also determined representative ages and mean metallicities of the cluster surrounding fields. We refer to 'representative age' as the age of the most numerous stellar population along the line-of-sight younger than 4.5 ± 1 Gyr (see Section 2). The surrounding field of a cluster was delimited as the region extending from a circle centred on the cluster and with an inner radius of 300 pixels extending out to the boundary of the CCD field. We derived ages from the δT_1 index, calculated by determining the difference in the T_1 magnitude of the RGC and the MS TO in field CMDs. We assigned to the TO T_1 magnitude an uncertainty three times that typical of the photometry at the TO level, i.e. $\langle \sigma_{\rm TO} \rangle = 0.10$ mag. Since field CMDs are obviously composed of MSs of different stellar populations, we derived δT_1 values for the MS with the TO containing the largest concentration of stars. We assumed that the observed MS is a result of the superposition of MSs with different TOs (ages) and constant luminosity functions. Hence, the difference between the number of stars of two adjacent magnitude intervals gives the intrinsic number of stars belonging to the faintest interval. Consequently, the biggest difference is directly related to the most populated TO. To find this maximum value, we counted the number of stars in bins of 0.25 mag along field MSs. This was accomplished by tracing lower and upper envelopes shifting the expression:

$$T_1 = 6.7(C - T_1 - \alpha) + 20.7$$

by -0.2 mag (bluewards) and $+0.2$ mag (redwards) in $C - T_1$, respectively. In the above equation, α is a constant equal to 0.0

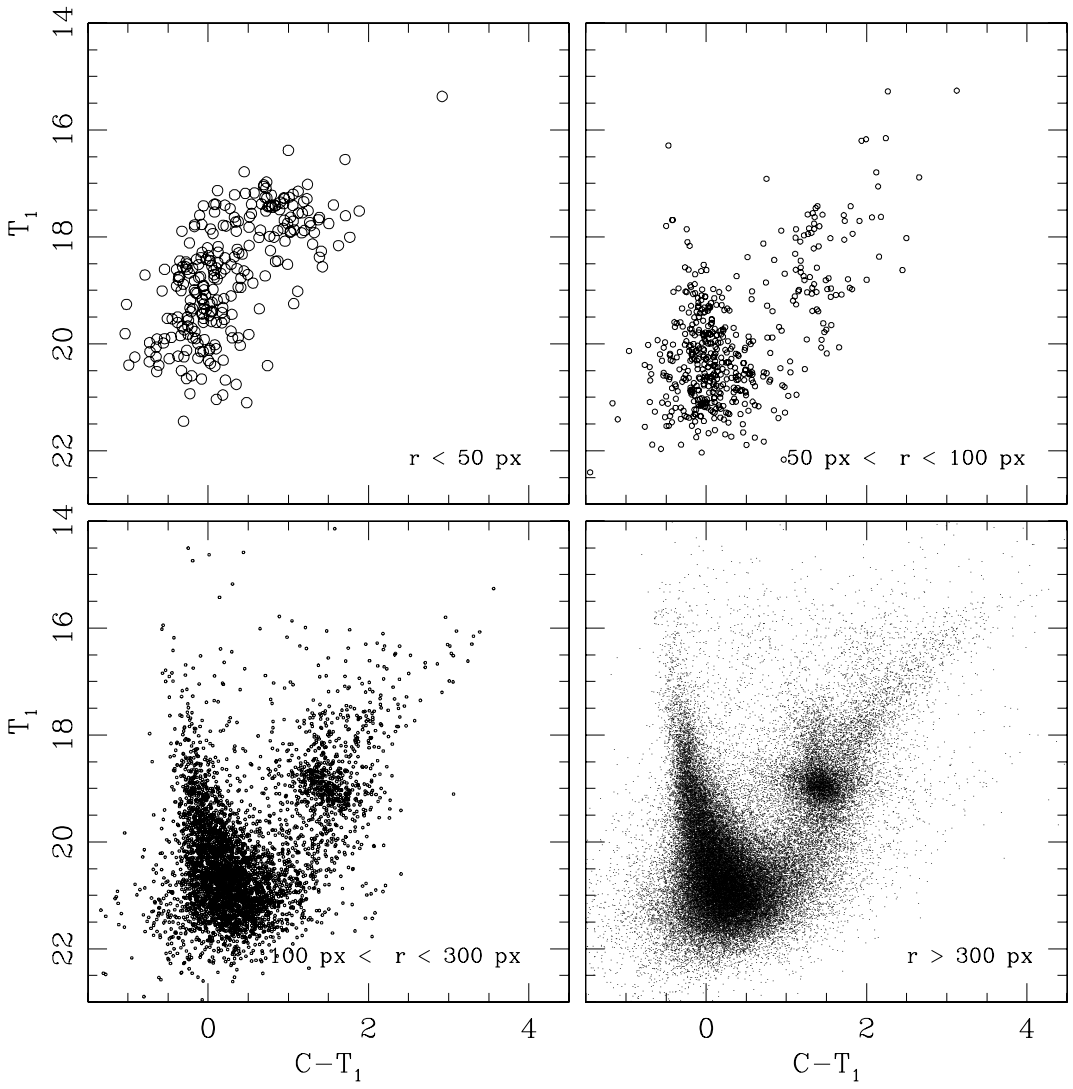

Figure 7. Washington T_1 versus $C - T_1$ CMDs for measured stars in the NGC 294 cluster field. Extraction radii in pixels are given in each panel.

(B 34, IC 1611, NGC 376) or 0.1 (NGC 256, 265, 294). We then derived ages from the δT_1 values using equation (4) of Geisler et al. (1997) and these are presented in Table 8. Since we estimated $\sigma(\delta T_1)$ = 0.20 mag, the uncertainty in the age values is of the order of 0.2–0.3 Gyr.

Finally, mean metallicities for the cluster surrounding fields were also obtained using the $[M_{T_1}, (C-T_1)_o]$ plane with the standard giant branches (SGBs) of Geisler & Sarajedini (1999). They demonstrated that the metallicity sensitivity of the SGBs (each giant branch corresponds to an isoabundance curve) is three times higher than that of the *V*, *I* technique (Da Costa & Armandroff 1990) and that, consequently, it is possible to determine metallicities three times more precisely for a given photometric error. However, the SGBs were defined mainly by using globular clusters older than 10 Gyr. In view of the well-known age–metallicity degeneracy, it is important to examine as closely as possible the effect of applying such a calibration based on very old objects to much younger clusters. Geisler et al. (2003) explored this effect empirically by comparing the differences in $(C - T_1)_o$ to the theoretical isochrones of LS. The result is presented in their fig. 6. They recommend using isochrone metallicities for clusters younger than 2 Gyr.

We then followed the standard SGB procedure of entering absolute M_{T_1} magnitudes and intrinsic $(C - T_1)_o$ colours for each field into fig. 4 of Geisler & Sarajedini to obtain by interpolation metal abundance values ([Fe/H]) to which we added the appropriate age correction, using the δT_1 ages we derived. The derived mean metallicities for the surrounding fields are listed in Column 6 of Table 8. Note that the field RGBs (see Figs 4 to 9, bottom right panels) are very well populated in general and show a significant colour (age) spread at a given magnitude, although it is difficult to tell how much of the observed spread is due to age spread and how much to metallicity spread. Here, we have simply given the mean metal abundance derived from the above analysis. We could determine mean metallicities to about 0.2 dex including all error sources.

5 ANALYSIS AND DISCUSSION

We determined fundamental properties for a sample of six SMC clusters: all of them are located within a radius of one degree from the SMC centre and five of them were found to be $\ll$1 Gyr (only B 34 is an $\sim$1 Gyr old cluster), allowing us to thus improve our knowledge of the late chemical evolution in the SMC inner disc.

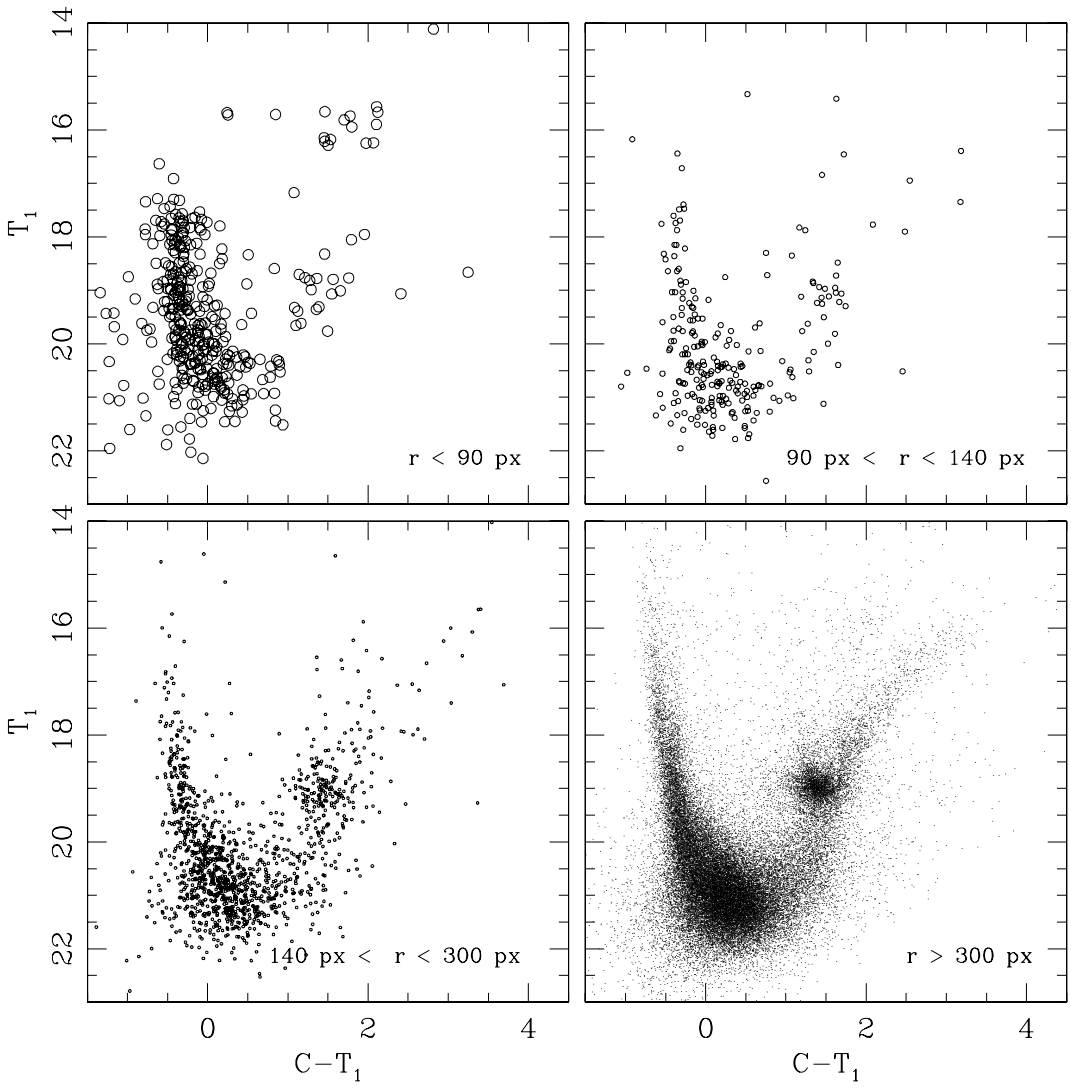

Figure 8. Washington T_1 versus $C - T_1$ CMDs for measured stars in the IC 1611 cluster field. Extraction radii in pixels are given in each panel.

Previous studies found in the literature related to the present cluster sample are those of Pietrzyński & Udalski (1999), de Oliveira et al. (2000), Ahumada et al. (2002) and Chiosi et al. (2006). These authors alternatively used integrated spectra of the clusters, Digitized Sky Survey images obtained from photographic plates or CMDs from the OGLE II photometric survey (Udalski et al. 1998). Most of these studies have one or two distinct clusters in common with our sample, and show some important differences between their values and our results in the derived ages and reddening estimates. For example, both Pietrzyński & Udalski and Chiosi et al. used the same OGLE data and estimated an age for NGC 265 of 100 and 250 Myr, respectively, while Ahumada et al. found a younger value of 50 Myr. Our age estimate for this cluster is 250 Myr. We found excellent agreement for the ages estimated by de Oliveira et al. for the two clusters in common, IC 1611 and NGC 376 (100 and 25 Myr). Conversely, the largest age difference between our values and those published by the mentioned authors occurs for B 34, for which we estimated twice the age derived by Chiosi et al. We believe that an additional advantage of the present results consists in having determined homogeneously the ages and colour excesses. Previous works employed a variety of procedures. However, further studies of the properties of these clusters are certainly warranted.

We have now studied the chemical enrichment of the SMC inner disc using ages and metallicities of 42 star clusters, put on to a homogeneous scale (Piatti et al. 2002, 2005a,b), including our present sample. For the spatial distributions, we adopted an elliptical framework instead of a spherical one, in order to reflect more meaningfully the flattening of the galaxy. Fig. 11 shows, besides the SMC Bar represented by a straight line, two ellipses centred at the SMC optical centre (cross) with their major axes aligned with the Bar. This reference system – with one of its axes parallel to the SMC Bar and the other one perpendicular to that – appears more appropriate for describing the cluster age and metallicity distributions than that with axes parallel to the right ascension and declination directions. We adopted a b/a ratio of $1/2$. The semimajor axes of the ellipses drawn in the figure have radii of 2° and 4°, respectively. Fig. 11 finally shows the positions of the 36 additional clusters and those of the six clusters studied here relative to the SMC optical centre – assumed to be at: $00^{\rm h}52^{\rm m}45^{\rm s}$, $-72^\circ49'43''$ (J2000) (Crowl et al. 2001) – drawn with open circles and crossed boxes, respectively. For completeness purposes, we included in the last column

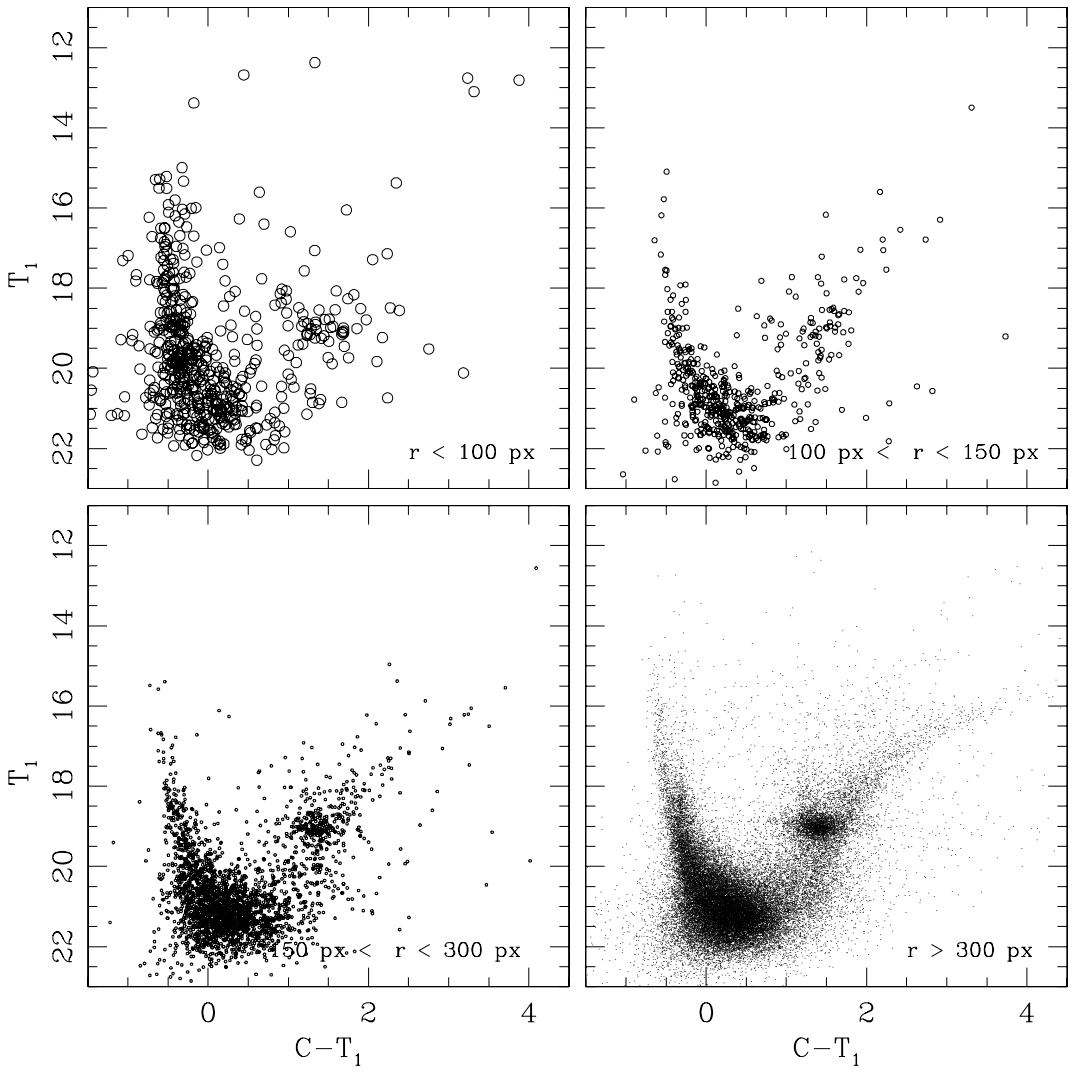

Figure 9. Washington T_1 versus $C - T_1$ CMDs for measured stars in the NGC 376 cluster field. Extraction radii in pixels are given in each panel.

Table 8. Fundamental parameters of SMC clusters.

Name	$E(B-V)_{\rm BH}$ (mag)	$\rm Age_{cluster}$ (Myr)	$\delta T_{1\rm field}$ (mag)	$\rm Age_{field}$ (Gyr)	$\langle$[Fe/H]$\rangle\,^{a}_{\rm field}$	R (°)
B 34	0.14	1200 ± 300	1.0	1.4	−0.95	0.60
NGC 256	0.05	160 ± 70	0.7	1.2	−0.60 to −1.10	0.84
NGC 265	0.05	250 ± 120	0.7	1.2	−0.60 to −1.10	0.76
NGC 294	0.06	320 ± 150	0.7	1.2	−0.95	0.55
IC 1611	0.15	100 ± 40	0.7	1.2	−0.95	0.72
NGC 376	0.14	25 ± 10	1.7	2.1	−0.80	0.82

[a] Metallicities were corrected according to fig. 6 of Geisler et al. (2003) (see Section 4 for details).

of Table 8 the calculated deprojected cluster distances *R*. Note that all of the studied clusters are located within one degree of the SMC centre.

In order to examine how cluster ages and metallicities vary in terms of the distance from the SMC centre, we computed for each cluster the value of the semimajor axis (a) that an ellipse would have if it were centred at the SMC centre, had a b/a ratio of $1/2$ and one point of its trajectory coincided with the cluster position. We plotted the obtained semimajor axes versus cluster ages and metallicities in Figs 12 and 13, respectively, wherein the present studied clusters and those from the literature are represented by open triangles and boxes, respectively. There is a clear trend, in the sense that the closer a cluster is to the centre of the galaxy, the younger it is, with some dispersion (Piatti et al. 2005a), supporting the results of Noel et al. (2006). A weaker tendency is seen in Fig. 13, suggesting that the more metal-poor a cluster, the more distant it is from the SMC centre. Note that in the outer disc – defined as the portion of the SMC disc with $a \geqslant 3\overset{\circ}{.}5$ – clusters have [Fe/H] $\leqslant$

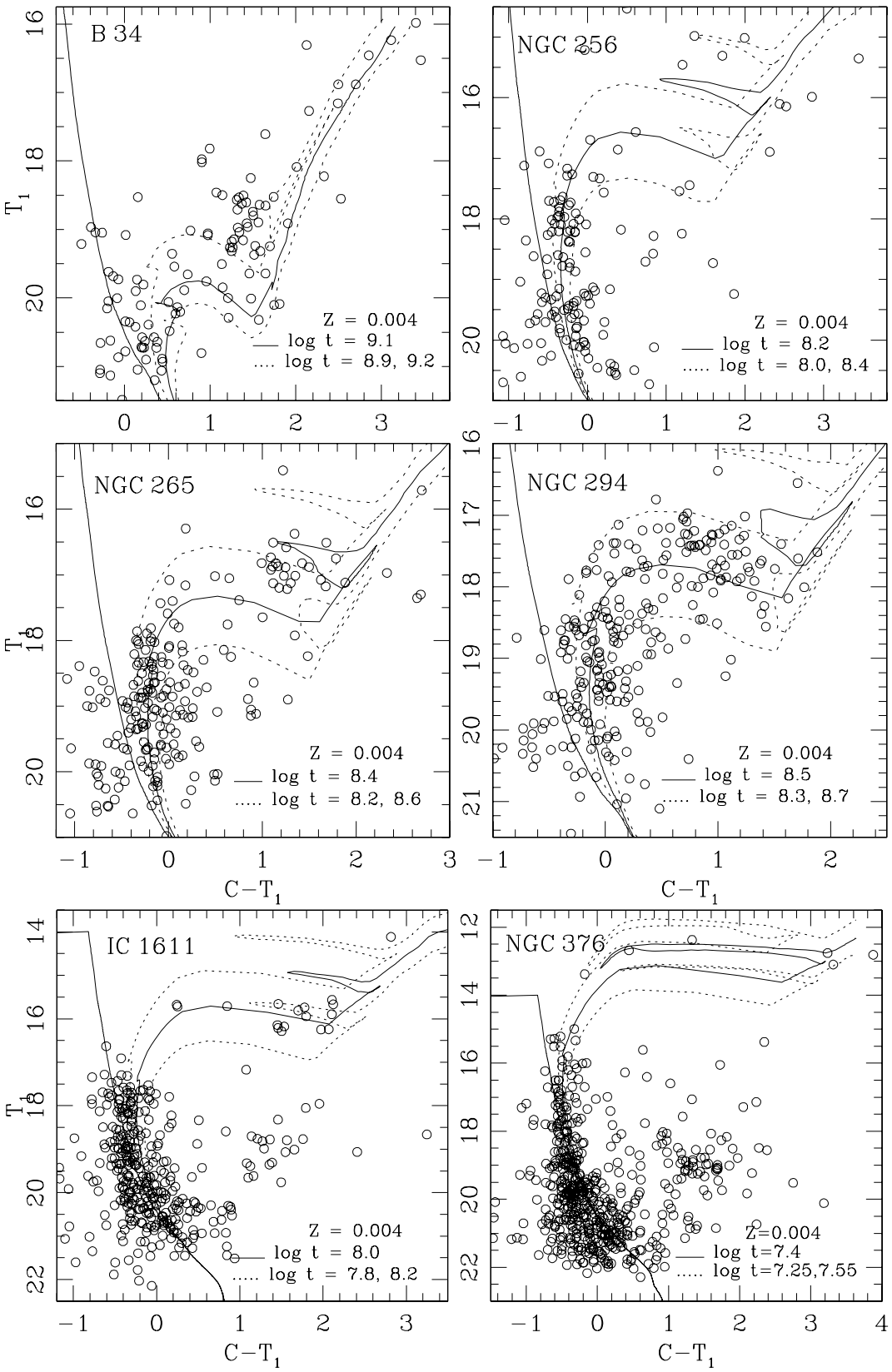

Figure 10. Washington T_1 versus $C - T_1$ CMDs for star clusters. Isochrones from Lejeune & Schaerer (2001), computed taking into account overshooting, are overplotted. The zero-age main sequence is also shown for the sake of completeness.

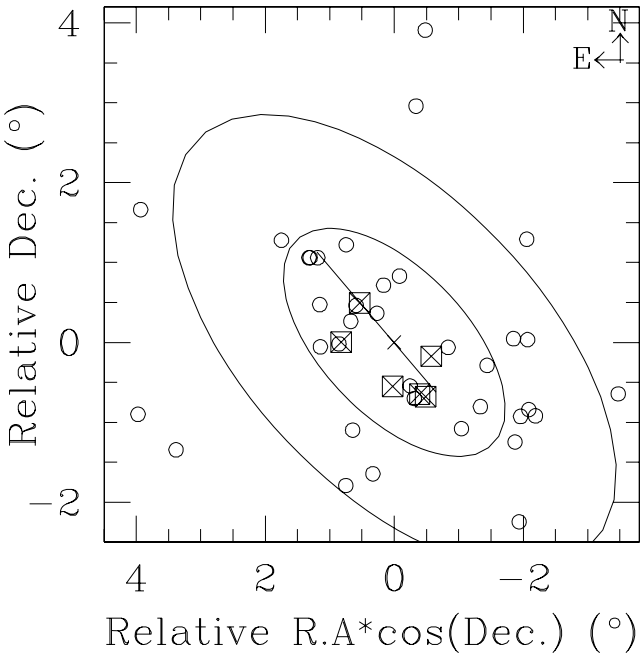

Figure 11. The position of the six studied cluster fields (crossed boxes) in relation to the SMC Bar (straight line) and optical centre (cross). Clusters included in Piatti et al. (2002, 2005a,b) are also shown as open circles.

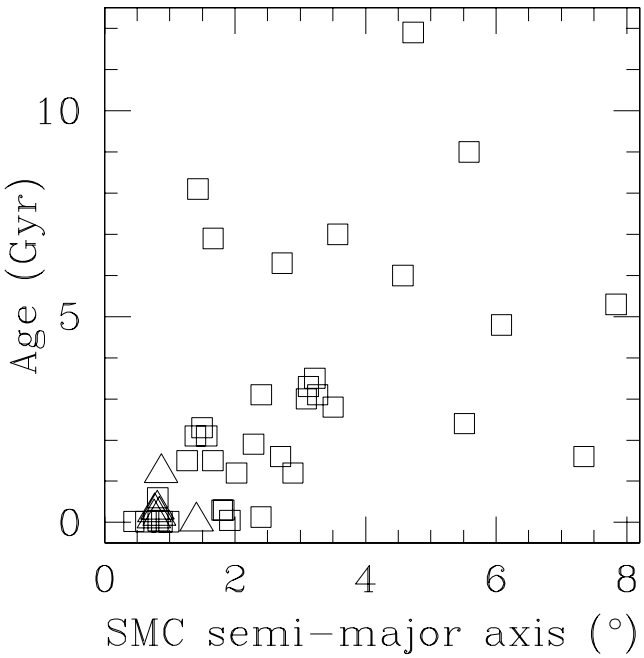

Figure 12. Cluster ages versus semimajor axes of ellipses with $b/a = 1/2$, centred at the SMC optical centre, aligned along the SMC Bar, that pass through the cluster positions. Open triangles and boxes, respectively, represent the six studied and the 36 literature clusters.

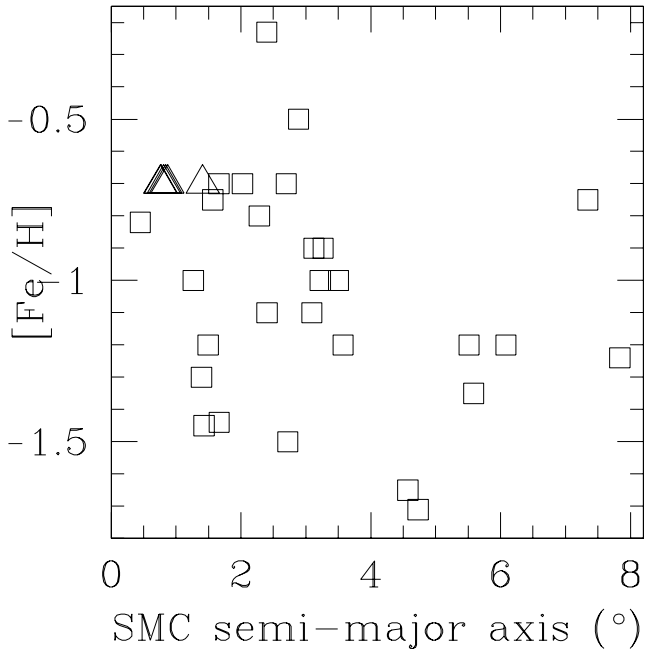

Figure 13. Cluster metallicity versus semimajor axes of ellipses with $b/a = 1/2$, centred at the SMC optical centre, aligned along the SMC Bar, that pass through the cluster positions. Symbols are as in Fig. 12.

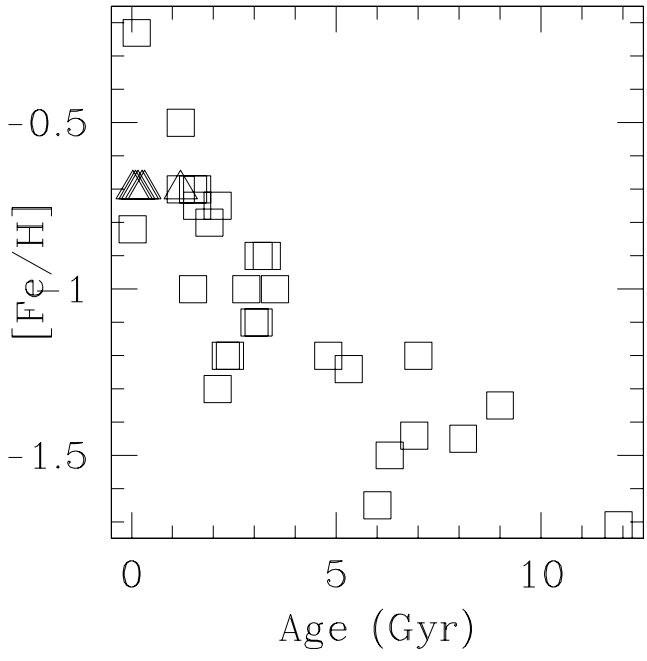

Figure 14. Age–metallicity relationship for star clusters in the SMC. Symbols are as in Fig. 12.

-1.2 with only one exception, while the inner disc is shared by both metal-poor and metal-rich clusters, the average metallicity being clearly larger than that for the outer disc. However, all the clusters with [Fe/H] > -1.2 in the inner disc were formed during the last 4 Gyr, whereas the metal-poor ones are as old as those in the outer disc (see Fig. 14). Consequently, the abundance gradient seems to reflect the combination between an older and more metal-poor population of clusters spread throughout the SMC and a younger and metal-richer one mainly formed in the inner disc. Both inferences are in very good agreement with the bursting scenario of cluster formation (Bekki et al. 2004; Piatti et al. 2005b), producing clusters from the outermost regions to the innermost ones in the inner SMC disc. Chiosi et al. (2006), who studied in detail the cluster distribution using a H I map, found a good correlation between the bursts in

cluster and field star formation similar to that found by Piatti et al. (2005a). Again, much further and more detailed work is needed to clarify and quantify these suggested trends.

Concerning the characteristics of the most numerous population of field stars, we found that the representative age of the fields in the inner SMC disc resulted to be 1.2 Gyr or somewhat older, and that the representative field ages are not correlated with the cluster ages. In fact, both young and intermediate-age clusters are superimposed on to intermediate-age fields, indiscriminantly. The youngest population of field stars have mean metallicities of ~ -0.9 dex, while clusters with similar ages are at least 0.3 dex more metal-rich (Piatti et al. 2005b, see their fig. 6). We interpret this result as evidence that most field stars are formed either from remnant gas clouds from star cluster formation or from disrupted clusters, in agreement with the scenario of Chandar et al. (2006).

6 SUMMARY

We have used the 0.9-m telescope at CTIO to obtain CCD imaging of a number of star clusters and their surrounding fields in the SMC as part of a continuing project. Here, we have presented the CMDs of B 34, NGC 256, NGC 265, NGC 294, IC 1611 and NGC 376 in the Washington photometric system. The CMDs are used to estimate ages for the clusters and metallicities and ages for the fields against which they are projected. Combining these results with those from our previous papers, we draw the following conclusions. There is a general tendency for the inner regions of the SMC to harbour younger clusters as compared to its outer regions. Furthermore, there is a tendency for the mean metallicity and its dispersion to be greater inside 4° of the SMC's centre as compared to outside this radius. In general, we find little correlation between the ages of the clusters and those of the field stars at the same location. These results clearly need to followed-up with more observations to confirm their robustness.

ACKNOWLEDGMENTS

This work was partially supported by the Argentinian institutions CONICET and Agencia Nacional de Promoción Científica y Tecnológica (ANPCyT). This work is based on observations made at CTIO, which is operated by AURA, Inc., under cooperative agreement with the NSF. We appreciate the valuable comments and suggestions of the anonymous reviewer, which helped us to improve the manuscript. We would like to thank the SMARTS consortium for their help and proficiency in obtaining part of these data. DG gratefully acknowledges support from the Chilean *Centro de Astrofí sica* FONDAP No. 15010003.

REFERENCES

Abraham R. G., 1999, in Barnes J. E., Sanders D. B., eds, Proc. IAU Symp. 186, Galaxy Interactions at Low and High Redshift. Kluwer, Dordrecht, p. 11
Ahumada A. V., Clariá J. J., Bica E., Dutra C. M., 2002, A&A, 393, 855
Bekki K., 2006, in Elmegreen B. G., Palous J., eds, Proc. IAU Symp. 237, Triggered Star Formation in a Turbulent ISM. Cambridge Univ. Press, Cambridge, p. 63
Bekki K., Couch W. J., Beasley M. A., Forbes D. A., Chiba M., Da Costa G. S., 2004, ApJ, 610, L93
Bica E., Schmitt H. R., 1995, ApJS, 101, 41
Burstein D., Heiles C., 1982, AJ, 87, 1165 (BH)
Canterna R., 1976, AJ, 81, 228
Chandar R., Fall S. M., Whitmore B. C., 2006, ApJ, 650, L111
Chiosi E., Vallenari A., Held E. V., Rizzi L., Moretti A., 2006, A&A, 452, 179
Cioni M. R., van der Marel R. P., Loup C., Habing H. J., 2000, A&A, 359, 601
Crowl H. H., Sarajedini A., Piatti A. E., Geisler D., Bica E., Clariá J. J., Santos J. F. C. Jr, 2001, AJ, 122, 220
Da Costa G. S., Armandroff T. E., 1990, AJ, 100, 162
de Oliveira M. R., Dutra C. M., Bica E., Dottori H., 2000, A&A, 146, 57
Font A. S., Johnston K. V., Bullock J. S., Robertson B. E., 2006, ApJ, 638, 585
Geisler D., 1996, AJ, 111, 480
Geisler D., Sarajedini A., 1999, AJ, 117, 308
Geisler D., Bica E., Dottori H., Clariá J. J., Piatti A. E., Santos J. F. C., Jr, 1997, AJ, 114, 1920
Geisler D., Piatti A. E., Bica E., Clariá J. J., 2003, MNRAS, 341, 771
Girardi L., Bertelli G., Bressan A., Chiosi C., Groenewegen M. A. T., Marigo P., Salasnich B., Weiss A., 2002, A&A, 391, 195
Grocholski A. J., Cole A. A., Sarajedini A., Geisler D., Smith V. V., 2006, AJ, 132, 1630
Harris J., Zaritsky D., 2004, AJ, 127, 1531
Hodge P. W., Wright F. W., 1974, AJ, 79, 858
Kron G. E., 1956, PASP, 68, 125
Lauberts A., 1982, ESO/Uppsala Survey of the ESO (B) Atlas. ESO, Garching bei Munchen
Lejeune T., Schaerer D., 2001, A&A, 366, 538 (LS)
Lejeune T., Cuisinier F., Buser R., 1997, A&AS, 125, 246
Lejeune T., Cuisinier F., Buser R., 1998, A&A, 287, 803
Lindsay E. M., 1958, MNRAS, 118, 172
Matteucci A., Ripepi V., Brocato E., Castellani V., 2002, A&A, 387, 861
Mighell K. J., Sarajedini A., French R. S., 1998, AJ, 116, 2395
Miley G. K. et al., 2006, ApJ, 650, L29
Navarro J., Frenk C., White S., 1997, ApJ, 490, 493
Noel N. E. D., Gallart C., Costa E., Mendez R. A., 2006, Rev. Mex. Astron. Astrofis., 26, 76
Pagel B. E. J., Tautvaišienė G., 1998, MNRAS, 299, 535
Piatti A. E., Santos J. F. C., Jr, Clariá J. J., Bica E., Sarajedini A., Geisler D., 2001, MNRAS, 325, 792
Piatti A. E., Sarajedini A., Geisler D., Bica E., Clariá J. J., 2002, MNRAS, 329, 556
Piatti A. E., Bica E., Geisler D., Clariá J. J., 2003a, MNRAS, 344, 965
Piatti A. E., Clariá J. J., Ahumada A. V., 2003b, MNRAS, 340, 1249
Piatti A. E., Clariá J. J., Ahumada A. V., 2003c, MNRAS, 346, 390
Piatti A. E., Clariá J. J., Ahumada A. V., 2004a, A&A, 418, 979
Piatti A. E., Clariá J. J., Ahumada A. V., 2004b, A&A, 421, 991
Piatti A. E., Santos J. F. C., Jr, Clariá J. J., Bica E., Ahumada A. V., Parisi M. C., 2005a, A&A, 440, 111
Piatti A. E., Sarajedini A., Geisler D., Seguel J., Clark D., 2005b, MNRAS, 358, 1215
Pietrzyński G., Udalski A., 1999, Acta Astron., 49, 157
Pietrzyński G., Udalski A., Kubiak M., Szymański M., Woźniak P., Zebruń K., 1998, Acta Astron., 48, 175
Schlegel D. J., Finkbeiner D. P., Davis M., 1998, ApJ, 500, 525 (SFD)
Searle L., Zinn R. J., 1978, ApJ, 225, 357
Stetson P. B., 1994, PASP, 106, 250
Stetson P. B., Davis L. E., Crabtree D. R., 1990, in Jacoby G. H., ed., ASP Conf. Ser. Vol. 8, CCDs in Astronomy. Astron. Soc. Pac., San Francisco, p. 289
Udalski A., Szymanski M., Kubiak M., Pietrzynski G., Wozniak P., Zebrun K., 1998, Acta Astron., 48, 147

SUPPLEMENTARY MATERIAL

The following supplementary material is available for this article.

Table 2. CCD CT1 data of stars in the field of B 34.
Table 3. CCD CT1 data of stars in the field of NGC 256.

Table 4. CCD CT1 data of stars in the field of NGC 265.
Table 5. CCD CT1 data of stars in the field of NGC 294.
Table 6. CCD CT1 data of stars in the field of IC 1611.
Table 7. CCD CT1 data of stars in the field of NGC 376.

This material is available as part of the online article from: http://www.blackwell-synergy.com/doi/abs/10.1111/j.1365-2966.2007.11604.x

(This link will take you to the article abstract.)

Please note: Blackwell Publishing are not responsible for the content or functionality of any supplementary materials supplied by the authors. Any queries (other than missing material) should be directed to the corresponding author for the article.

This paper has been typeset from a TEX/LATEX file prepared by the author.